ORIGINAL RESEARCH PAPER

Optimization of fuel ratio in solution combustion method for fabrication of nickel aluminate spinel used in the esterification reaction

Alireza Heydari [1], Ali Ahmadpour [1], Hamed Nayebzadeh [2,*], Naser Saghatoleslami [1,2], Amir-Hossein Azmoon [1]

[1]Department of Chemical Engineering, Faculty of Engineering, Ferdowsi University of Mashhad, Mashhad, Iran
[2]Esfarayen University of Technology, Esfarayen, North Khorasan, Iran
[3]Department of Petroleum Engineering, Eqbal Institute of Higher Education, Mashhad, Iran

ABSTRACT

In this study, the solution combustion method as a simple, fast, and cost-effective method was utilized for the fabrication of spinel nickel aluminate as a stable material to use in the esterification reaction. The effect of fuel amount (urea) as an important parameter of the solution combustion method on the structure, properties, and performance of the sample was evaluated. The results of characterization analyses revealed the highest crystallinity with the desired diffusion of nickel cations in alumina lattice was obtained for the sample prepared at a fuel ratio of 1.5. Moreover, a large pore size without any agglomerated particle was observed because of releasing a huge amount of gases and high reaction temperature formed during the combustion reaction. The sulfate groups were impregnated on the $NiAl_2O_4$ surface to increase the sample activity in the esterification reaction. The chelating bidentate structure can confirm suitable bonding of sulfate groups with the surface of $NiAl_2O_4$. Evaluating the nanocatalyst activity in the esterification reaction of oleic acid confirmed the high activity of $SO_4^{2-}/NiAl_2O_4$ nanocatalyst (94.2%) at the optimum condition of 120℃, 6 molar ratio of methanol/oleic acid, 3 wt.% of catalyst, and 3 h reaction time. In addition, stability assessment of nanocatalyst with and without post-treatment after each run exhibited that the porosity blocking and poisoning of the surface functional group were the major reasons for reducing the activity of the nanocatalyst. This activity was increased more than two times when the nanocatalyst was treated by washing and calcination (five cycles) after each use.

Keywords: Catalyst Post-Treatment; Esterification; Fuel-To-Oxidizer Ratio; Solution Combustion Method; Spinel Nickel Aluminate

© 2019 Published by Journal of Nanoanalysis.

INTRODUCTION

Despite the widespread use of biodiesel as one of the best biofuels in the current engines and its broad production around the world, some drawbacks in its production process have been a matter of debate. Biodiesel, as called fatty acid methyl ester (FAME), is usually produced via transesterification of triglycerides in vegetable oil with methanol using a homogeneous alkaline catalyst (e.g., KOH and NaOH). However, the drawbacks involved in producing this biodiesel (e.g., food security, deforestation, water consumption during the purification process, and release of alkaline wastewater) have been the subject of intense research.

In the second and third generations of biodiesel production, the researchers have suggested low-cost oils such as waste cooking oil [1] and non-edible

oils [2-4]. Although this feedstock was suggested for overcoming the aforementioned issues, a high level of free fatty acids (FFAs) of non-edible oils lead to another problem; i.e., the formation of soap [5]. Some researchers suggested a two-step process containing esterification of FFA using homogeneous acid catalyst before conventional transesterification reaction. This process not only solves the drawbacks of water demand of biodiesel production process, but also makes some disadvantage such as corrosion of equipment and acid wastewater. Therefore, fabrication of various heterogeneous catalysts has become the subject of intensive research to overcome the problems.

Many solid acid catalysts, especially sulfated transition metal oxides, have been studied in the esterification and transesterification reactions [6, 7]. Nowadays, mixed metal oxides receive attention because of their both Lewis (anion) and Brønsted acid sites (cations), which provide necessary catalytic sites for performing simultaneous esterification and transesterification processes [8]. Also, mixing transition metal oxides with alumina has been the subject of intense research [9-11].

Nuithitikul et al. [12] compared the activity of SO_4^{2-}/Al_2O_3-SnO_2 and SO_4^{2-}/Co_2O_3-SnO_2 in the esterification reaction. The results revealed that SO_4^{2-}/Al_2O_3-SnO_2 had a higher activity. They also reported that an increase in the alumina in SO_4^{2-}/SnO_2 increased the stability of the catalyst [13]. Roh et al. [14] studied the activity of Ni catalyst supported on MgO-Al$_2$O$_3$ and presented that increasing the Ni component, due to the formation of NiO species, accelerates the reaction rate. Moreover, Xu et al. [15] presented the effect of loading Ni cations on the activity of Mo-Al$_2$O$_3$. Wijayanti and Duangchan [16] investigated the effect of nickel promoter on solvent-free sulfated zirconia catalyst for the esterification of acetic acid. They described that the addition of nickel contributed to the increase of sulfur content that bonded with nickel, an increase in thermal stability of the catalysts, and formation of additional sulfate groups, and thus better catalytic performance. Keskin et al. [17] also confirmed the effect of nickel component as metallic fuel additive on the reduction of fuel consumption and emissions.

Technology developments increase the demand for materials with unique properties. The spinel compounds with the molecular formula of AB$_2$O$_4$ – where A is divalent cations such as Cu, Mg, Ni, Co, Ba, Sr, and B are trivalent cations such as Fe, Al, Mn,

and Cr – have been recently concerned because of their high resistance to thermal and chemical environment [18, 19]. Although some advantages of nickel as catalyst and additive have been reported in the production and combustion of biodiesel, there is a lack of study on the spinel structure (NiAl$_2$O$_4$). Spinel structure is formed with chemical routs by calcination at the high temperature (over 1000°C) and/or long time mechanical (milling) process (around 60 h) [11, 20]. Unlike the mentioned methods, solution combustion method is a quick and easy process for obtaining nanoscale powders with high purity, fine particle sizes, and usually a small aggregation and/or agglomeration particles [21]. This process contains a reaction between metal nitrate as oxidants and reducing reagents as called fuels such as urea, glycine, or other water-soluble carbohydrates. Several parameters can effect on the combustion reaction, with the type of fuel and fuel-to-oxidizer ratio (FOR) being the most important ones [22]. It has been reported that crystal phases, crystallinity, crystallite size, surface area, pore size, and morphology of a final product are generally controlled by adjusting the FOR [23, 24]. However, a limited number of studies have been conducted on using spinel nickel aluminate in the biodiesel production process.

In the present study, spinel nickel aluminate was prepared via a solution combustion method with different amounts of FOR followed back analysis of its crystalline phase, surface area, and morphology. Moreover, the sulfate groups were impregnated on the nickel aluminate as active phases to increase its activity for esterification reaction and the effect of reaction conditions were optimized using the best-sulfated nickel aluminate fabricated by optimum FOR. Finally, the reusability and stability of the nanocatalyst were examined.

MATERIALS AND METHODS
Catalyst preparation

The solution combustion synthesis method was utilized for fabrication of spinel NiAl$_2$O$_4$ with the initial solution contains nickel nitrate hexahydrate (Ni(NO$_3$)$_2$.6H$_2$O) and aluminum nitrate nonahydrate (Al(NO$_3$)$_3$.9H$_2$O) as an oxidizer and different amounts of urea as a reducer. Four types of samples were synthesized by mixing 1.94 g nickel nitrate and 5 g aluminum nitrate with 50 mL distilled water, adding a specific amount of urea based on the fuel-to-oxidizer ratio (ϕ) of 0.5, 1, 1.5, and 2. The amount of urea to ϕ = 1

corresponding to the stoichiometric compositions can be calculated as follows:

$$Ni(NO_3)_2.6H_2O + 2Al(NO_3)_3.9H_2O + 6.67CO(NH_2)_2$$

$$\rightarrow NiAl_2O_4 + 15H_2O + 6.67CO_2 + 10.67N_2 \qquad (1)$$
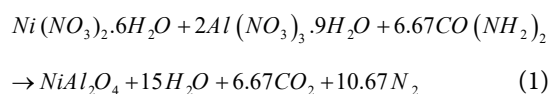
Each mixture was heated on a hot plate under stirring to evaporate the excess water and a viscose gel remained. To start the SCS, the gel was placed in an oven at 400℃. After boiling up the remained water, the combustion reaction was initiated with the extreme release of smoke, then igniting from a point and spreading to all mixtures. After subsiding the flame, the foam-like structure was obtained. Next, the samples were cooled at room temperature and labeled as $NiAl_2O_4$ ($\phi = 0.5$), $NiAl_2O_4$ ($\phi = 1$), $NiAl_2O_4$ ($\phi = 1.5$), and $NiAl_2O_4$ ($\phi = 2$).

In the next step, the sulfate group was impregnated on the surface of $NiAl_2O_4$ fabricated by the SCS method to improve its activity in the esterification reaction. For this purpose, 10 mL of 1 M H_2SO_4 aqueous solution was mixed with 1 g of spinel $NiAl_2O_4$ and 30 mL distilled water and refluxed for 3 h at 80℃ under mild magnetic stirring. Then, the mixture was placed in an oven at 110℃ for overnight to dry. Finally, the powder was calcined in the furnace at 550℃ for 3 h to obtain S/$NiAl_2O_4$ ($\phi = 0.5$), S/$NiAl_2O_4$ ($\phi = 1$), S/$NiAl_2O_4$ ($\phi = 1.5$), and S/$NiAl_2O_4$ ($\phi = 2$) nanocatalysts.

Catalyst characterization

The crystalline phase of the samples was determined by XRD analysis in a 2θ range of 10-80° using a UNISANTIS/XMP 300 by means of Cu K_α radiation operating at 45 kV and 80 mA along calculating their crystalline size using Scherer equation. The quality of nanocatalyst preparation via combined impregnation-combustion method was assessed by TG/DTA analysis at 50-1000℃ under air medium at a heating rate of 20℃ /min using an Evolution STA (SETARAM, France). The surface functional groups were detected by FTIR analysis in the range of 400-4000 cm⁻¹ using SHIMADZU 4300 (Japan) spectrometer. The specific surface area, mean pore size, and pore volume of the nanocatalysts were measured by BET-BJH method using PHS-1020 (PHSCHINA, China) apparatus. Moreover, adsorption-desorption hysteresis and pore size distribution plots of samples were thoroughly discussed. The surface structure and morphology of the nanocatalysts were studied by FESEM analysis using MIRA3 FEG-SEM

(TESCAN, Czech Republic). The distribution of elements on the surface of the sample was quantified by the EDX technique using VEGA II Detector (Czech Republic, TESCAN). The acid strength of the solid acid nanocatalyst (H_0) as an important factor to assess the activity of a sample in the esterification reaction was determined using Hammett indicators. Afterward, 0.01 N Butyl-Amin solution was utilized for titration of a mixture containing 0.2 g catalyst, 10 mL methanol and 1 mL of Hammett indicators (Methyl red (H_0=4.8), p-Dimethylaminoazobenzene (H_0=+3.3), violet crystal (H_0=0.8), and dicinnamalacetone (H0 = -3.0, basic)) [25].

Esterification reaction

The esterification reaction was performed to assess the activity of sulfated spinel nickel aluminate nanocatalysts. The reaction was performed in a 100 mL stainless steel batch reactor poured with 20 g oleic acid ($C_{18}H_{34}O_2$, 9-octadecenoic acid) as one of the major FFA in the oils (edible and inedible oils), 0.6 g of catalyst (3 wt.%), and 25.8 mL of methanol (methanol-to-oleic acid molar ratio (MOR) of 9) [26]. The reaction was carried out at a thermocouple (Type K) and a magnetic stirrer. The esterification reaction was carried out at 120 ± 2℃, which was adjusted by a thermocouple (Type K), and a stirring rate of 600 rpm for 4 h. After cooling down the reactor to room temperature (when the reaction was done), the mixture was settled in a separating funnel and the top layer containing methyl oleate was separated from other materials of the mixture (i.e., water and catalyst). The yield of esterification reaction was determined based on reducing the acidity of oleic acid to methyl oleate by using titration a mixture containing 0.5 g of sample and 10 mL methanol with 0.1 M alcoholic (ethanol) potassium and phenolphthalein as an indicator [27].

RESULTS AND DISCUSSION

XRD analysis

The XRD patterns of spinel $NiAl_2O_4$ prepared by SCS method at the different fuel-to-oxidizer ratio ($\phi = 0.5$, 1, 1.5, and 2) are illustrated in Fig. 1. The results present that the crystallinity of the powder was increased by increasing the ϕ such that nickel cations were diffused in alumina lattice to form spinel $NiAl_2O_4$ (JCPDS No. 78-1601) due to increase the combustion reaction temperature and duration. It was reported that the temperature must
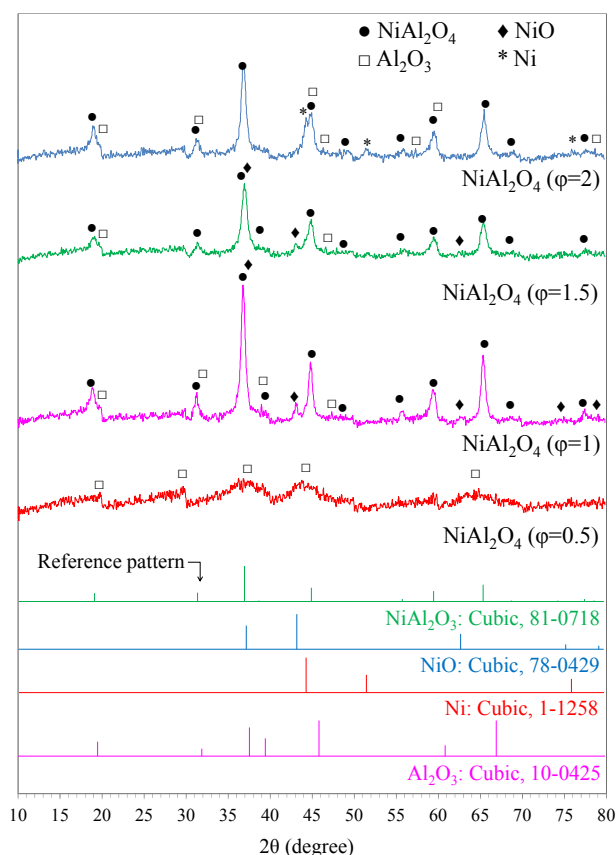
Fig. 1. The XRD patterns of NiAl$_2$O$_4$ spinel prepared using solution combustion method at different F/O ratio

exceed 1000℃ for nickel cations to diffuse through the early layer of aluminate lattice [28]. Moreover, the nickel oxide (JCPDS No. 71-1179) and alumina (JCPDS No. 9-0440) peaks can be detected for NiAl$_2$O$_4$ (ϕ = 1). By increasing the ϕ from the stoichiometric amount (ϕ = 1) to 1.5, the peaks of nickel oxide and alumina were sharply reduced. It can be related to well-bonding between nickel and aluminum cations to form spinel NiAl$_2$O$_4$ due to raising the combustion temperature.

However, Ni peaks were detected at a very high amount of ϕ. This result can be explained by two reasons; (1) an excessive increase in combustion temperature and duration and tendency of metal cations to make crystals apart from each other, and (2) release of a high amount of smoke from reaction medium that prevents diffusion of oxygen in the combustion medium for oxidizing the Ni to NiO [29]. Lead et al. [30] studied the formation of spinel NiAl$_2$O$_4$ via combustion method using glycine as fuel. They presented that excess amounts of glycine favor formation of NiO while Ni phases hinder the NiAl$_2$O$_4$ phase; this result is in agreement

with the results of the present study. Moreover, the formation of the alpha phase of alumina can prove the increase in the combustion reaction temperature by using fuel at a ratio of 2.

The XRD patterns of spinel NiAl$_2$O$_4$ promoted by the sulfate group are shown in Fig. 2. As shown in Fig. 2(a), due to less crystallinity of the support and no diffusion of nickel cations into alumina lattice, the nickel sulfate (JCPDS No. 76-0220) is the main structure of S/NiAl$_2$O$_4$ (ϕ = 0.5). In comparison, aluminum cations need the high calcination temperature to transform from amorphous to crystal form and make bands with sulfate groups. Therefore, aluminum sulfate peaks (Millosevichite, JCPDS No. 42-1428) with less intensity were observed. Overall, it is inferred that the calcination process affects the crystallinity of the sample to transform from amorphous to crystal.

When the sulfate groups were impregnated on the support with higher crystallinity, due to the diffusion of nickel cations in the alumina lattice, the aluminum sulfate peaks are the major peaks in the pattern of other samples. The support prepared
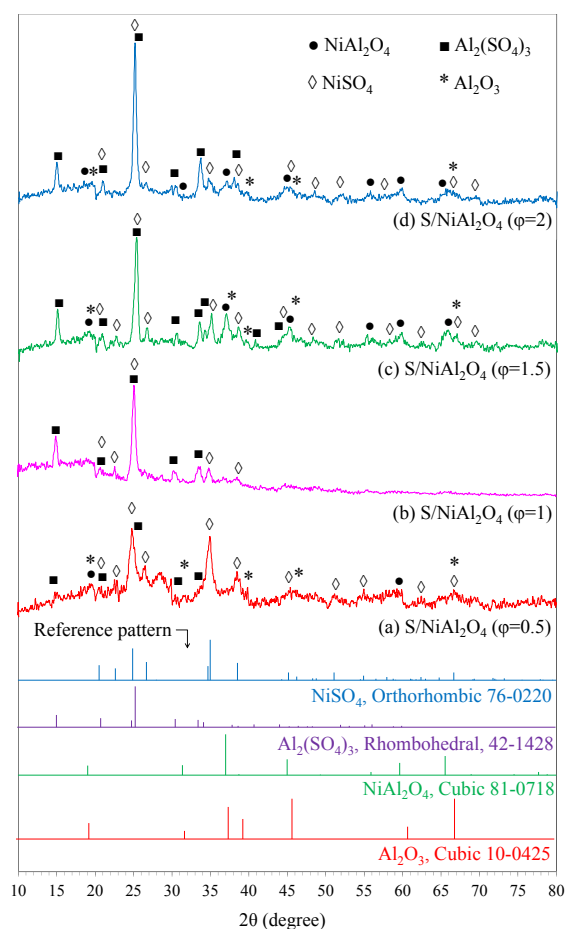
Fig. 2. The XRD patterns of sulfated $NiAl_2O_4$ nanocatalysts prepared by solution combustion method at different F/O ratio

by $\phi = 1$, which had the highest intensity of spinel crystals, presented lower peaks of nickel sulfate. It can be due to less bonding of sulfate groups to the surface, especially aluminum cations, to form sulfate aluminum. The supports prepared by $\phi > 1$ presented high intensity of aluminum sulfate and nickel sulfate along with $NiAl_2O_4$ peaks with lower intensity. Moreover, the number of these structures peaks is higher than those formed for $S/NiAl_2O_4$ ($\phi = 1$). Detail study of XRD plots of the samples prepared at $\phi > 1$ shows that $NiSO_4$ peaks are sharper for $S/NiAl_2O_4$ ($\phi = 1.5$) compared to $S/NiAl_2O_4$ ($\phi = 2$), probably because of their higher activity.

The relative crystallinity and crystallite size of the samples, which were determined based on the sharpest peak ($2\theta = 25.1°$), are listed in Table 1. The relative crystallinity was increased using a higher amount of fuel for preparation of $NiAl_2O_4$ as support due to an increase in the combustion reaction temperature and the increase in the number of materials transformed from amorphous

to crystal form. The crystalline size measured by Scherer equation presented that $S/NiAl_2O_4$ ($\phi = 1.5$) has the lowest crystalline size.

TG-DTA analysis

The TG-DTA plots of the samples are shown in Fig. 3. As can be seen, with a slight difference in weight loss and at different temperatures, all the studied samples have the same TG-DTA plots. The initial weight loss (50-200℃) is assigned to the elimination of physically adsorbed water on the surface of the catalyst [5, 31]. In the region of 200℃ to 600℃, non-significant weight loss was observed, which confirms the decomposition of the nitrate group of precursors [29]. In the third region (600-850℃), a significant weight loss was observed that can be explained by two peaks appeared in the DTA plots. The first weight loss with the sharp peak of DTA at around 740℃ is related to the decomposition of adsorbed sulfate ions to SO_2 [26]. Among the samples, $S/NiAl_2O_4$ ($\phi = 0.5$)

Table 1. Physicochemical properties of sulfated NiAl$_2$O$_4$ prepared by solution combustion method at different F/O ratio

Nanocatalyst	BET (m^2/g)	P$_V$ (cm^3)	P$_d$ (nm)	Acidity H_	Strength (mmol/g)	Relative Crystallinity[a]	Crystallite size[b] (nm)
S/NiAl$_2$O$_4$(F/O=0.5)	30.93	0.38	4.25	-0.3-0.8	0.95	43.9	-
S/NiAl$_2$O$_4$(F/O=1)	30.48	0.115	4.13	-0.3-0.8	1.28	51.2	16.9
S/NiAl$_2$O$_4$(F/O=1.5)	28.57	0.127	6.10	-0.3-0.8	1.52	68.9	16.3
S/NiAl$_2$O$_4$(F/O=2)	36.8	0.138	5.31	-0.3-0.8	1.54	100	20.3

a. Relative crystallinity: XRD relative peak intensity at 2θ = 25.1° for S/NiAl$_2$O$_4$.
b. Crystallite size estimated by Scherre's equation at 2θ = 25.1° for S/NiAl$_2$O$_4$.
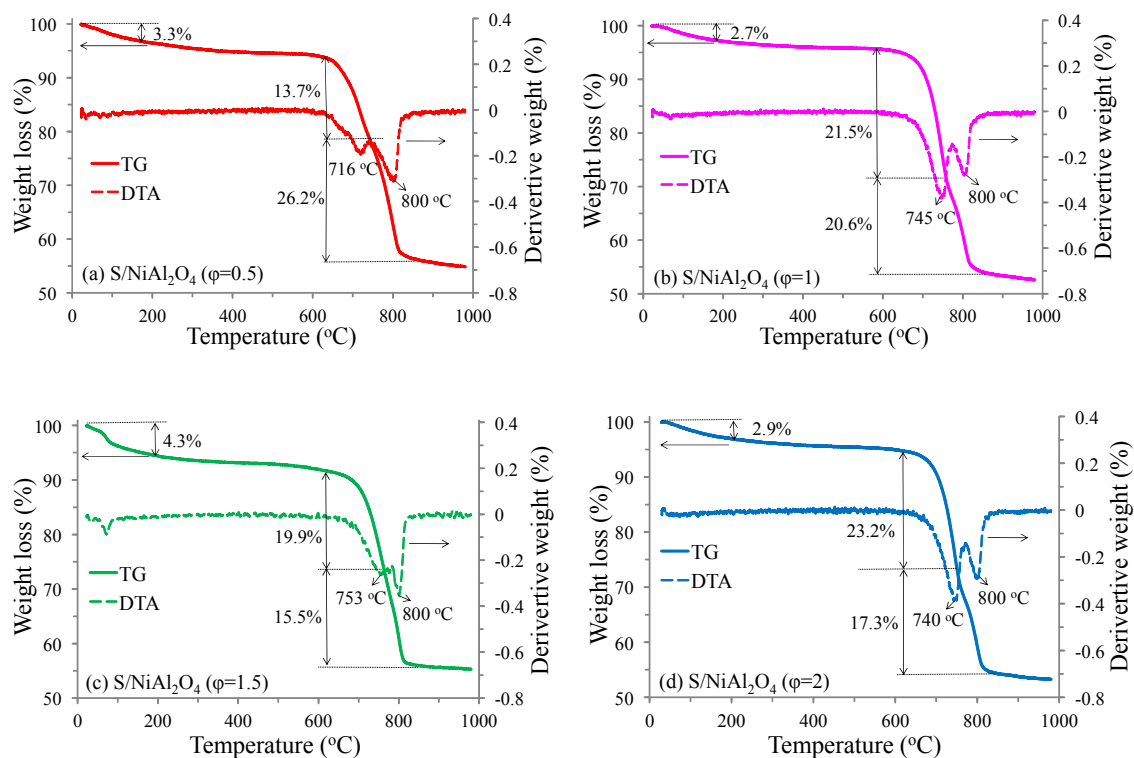

Fig. 3. TG/DTA plots of sulfated NiAl$_2$O$_4$ nanocatalyst prepared by solution combustion method at different F/O ratio

shows the lowest weight loss and earlier DTA peak, which is related to less crystallinity of this catalyst for bonding between sulfate group and surface of support and transformation of amorphous components to crystal form [5]. The second weight loss in this region is attributed to the diffusion of nickel cations into alumina lattice to form NiAl$_2$O$_4$ [32]. This result proves the good performance of the combustion reaction for the formation of spinel NiAl$_2$O$_4$ with the highest crystallinity at ɸ = 1.5. Moreover, the results reveal that the combustion reaction temperature is certainly higher than 800℃, because of which the nickel cations diffused through alumina lattice. In the final region (800-1000℃), negligible weight loss was observed, confirming the formation of NiAl$_2$O$_4$ and absence of amorphous structure.

FTIR analysis

The FTIR spectra of the samples are depicted in Fig. 4. All samples show similar FTIR spectrum with a slight difference in the intensity of the peaks. It confirms the formation of the bands (i.e., aluminum sulfate, nickel sulfate, and nickel aluminate) in all samples with different crystallinity level and strength. These results are in good agreement with XRD results. The metal cation-oxygen, such as Al-O, Ni-O, and Ni-O-Al were detected in the region below 1000 cm^{-1}. The Al-O bands appeared in the range of 500-650 cm^{-1} and 650-850 cm^{-1}, which corresponds to the vibration of AlO$_6$ and AlO$_6$, respectively. The Ni-O bands were observed in the range of 400-500 cm^{-1} [33]. The band around 830 cm^{-1} became broad for NiAl$_2$O$_4$ nanocatalyst prepared by ɸ>1, which suggests the formation of

nickel aluminate. Ragupathi et al. [34] reported that $NiAl_2O_4$ (Al–O–Ni frequencies appear in the range of 450–850 cm^{-1}) is formed as a mixture of the normal spinel (Al^{3+} ions in octahedral sites of AlO_6 groups) and the inverse spinel (Al^{3+} ions in octahedral AlO_6 and tetrahedral AlO_4 sites).

In addition to metal-O peaks, some strong peaks related to sulfate groups (symmetric and asymmetric vibration of S = O) appeared at 985 cm^{-1}, 1038 cm^{-1}, 1185 cm^{-1}, and 1320 cm^{-1}, which are attributed to chelating bidentate sulfate ions coordinated to Ni/Al cations [35, 36]. The broadband between 2800 and 3600 cm^{-1} and a band at 1640 cm^{-1} is respectively assigned to stretching and bending vibration of OH groups, which was physically adsorbed on the surface of
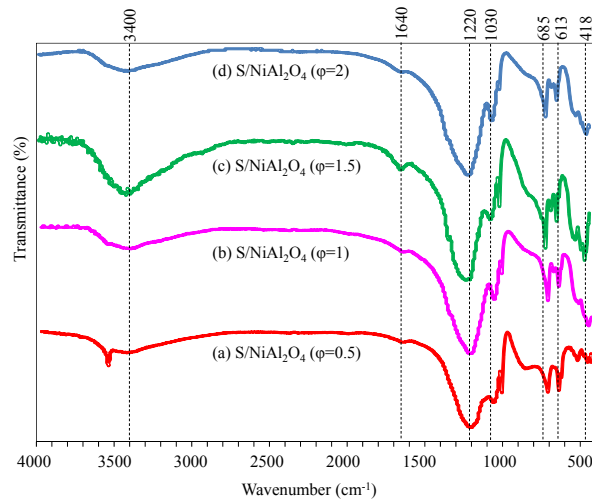

Fig. 4. FTIR spectra of sulfated $NiAl_2O_4$ nanocatalysts prepared by solution combustion method at different F/O ratio
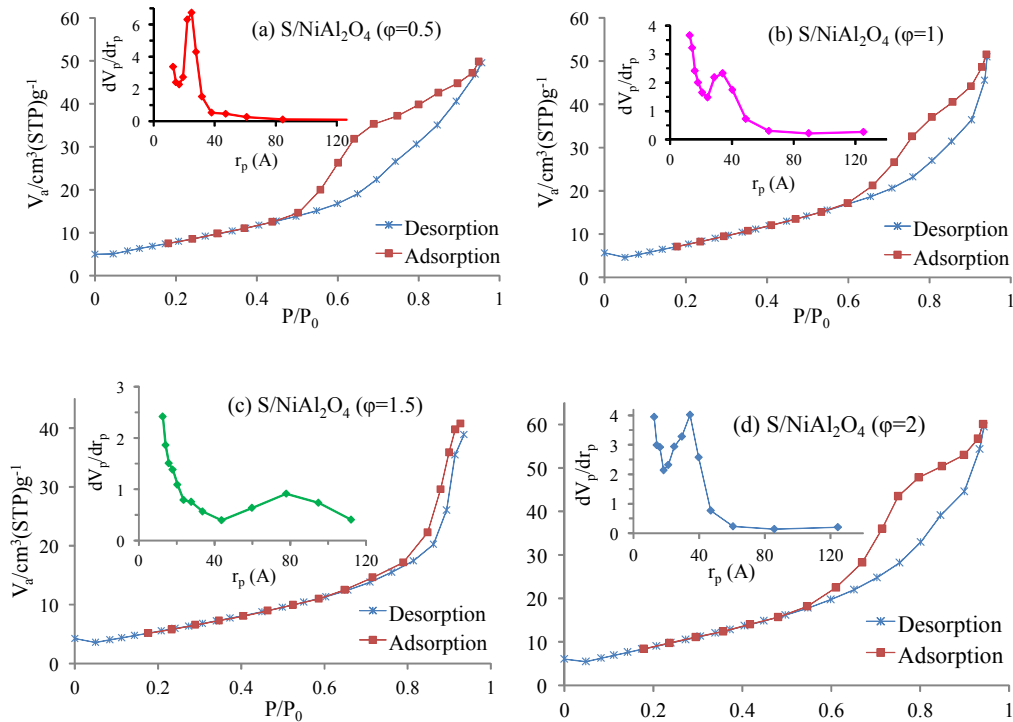

Fig. 5. N_2 adsorption-desorption hysteresis of sulfated $NiAl_2O_4$ prepared by solution combustion method at different F/O ratio

the nanocatalysts during compacting with KBr as pellets [37, 38].

BET-BJH and Basicity analysis

The hysteresis loops of the samples are illustrated in Fig. 5. The figure presents N$_2$ adsorption-desorption hysteresis of all samples in the classification of mesoporous materials (Type-IV isotherm) with type H2 at a relative pressure (P/P$_0$) of 0.6-1.0, except for S/NiAl$_2$O$_4$ (ϕ = 1.5) nanocatalyst [39]. These hysteresis loops are attributed to macroporous materials or non-porous materials possessing large interparticle voids, which in many cases the smaller pore acts as a neck (often referred to as an "ink-bottle" pore) [5, 40]. S/NiAl$_2$O$_4$ (ϕ = 1.5) nanocatalyst shows hysteresis of type H1, which is related to cylindrical and spherical pores [41]. These samples present a BET surface area of 28 to 37 m^2/g (Table 1). Among the studies samples, S/NiAl$_2$O$_4$ (ϕ = 2) has the highest BET surface area and S/NiAl$_2$O$_4$ (ϕ = 1.5) has the lowest.

An important parameter in the reaction containing reactants with large molecules such as transesterification reaction is the size of pores, especially when the samples have a similar surface area. Permeation of reactant inside the pores and availability of the internal surface area to facilitate the mass transfer of reactants to the active acidic sites of the heterogeneous catalyst play a major role on the activity of a catalyst [39]. According to Table 1, S/NiAl$_2$O$_4$ (ϕ = 1.5) nanocatalyst has the highest mean pore size (around two times of other samples), which is in good agreement with the results of pore size distribution (Fig. 5). Except for S/NiAl$_2$O$_4$ (ϕ = 1.5), other samples have similar pore size distribution, which can be related to their pore shape as explained based on their hysteresis loop.

The basicity of the samples as important parameters on the activity of a catalyst in the esterification reaction was measured by Hammett indicators methods and the results were presented in Table 1. All the studied samples have acidity in the range of -0.3 <H$_0$<0.8. As expected from other results, S/NiAl$_2$O$_4$ (ϕ = 1.5) and S/NiAl$_2$O$_4$ (ϕ = 2) have higher basicity due to their higher crystallinity, sulfate group bonded with surface and less amorphous structure.

FESEM analysis

The morphology of the samples prepared by different amount of urea during combustion reaction was assessed by FESEM analysis. The agglomerated and shapeless particles formed at ϕ = 0.5, which is related to less combustion temperatures to transform the materials from amorphous to crystal form. Although S/NiAl$_2$O$_4$ (ϕ = 0.5) has an unshaped structure, sulfate groups are uniformly dispersed on the surface of the support.
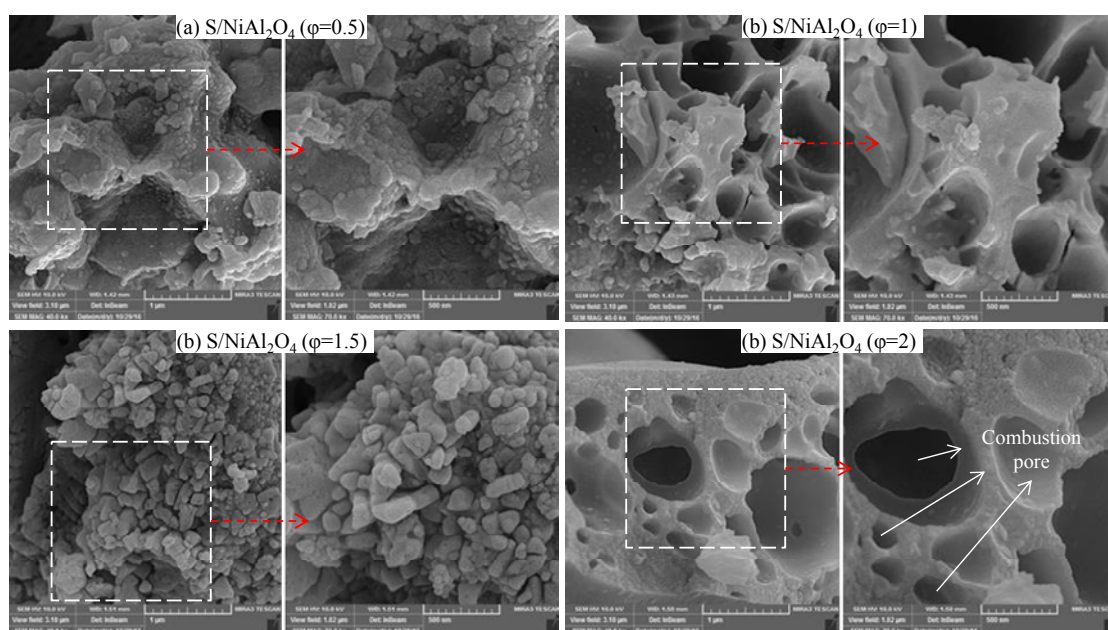

Fig. 6. FESEM images of sulfated NiAl$_2$O$_4$ prepared by solution combustion method at different F/O ratio

By increasing the fuel amount, the support shape was changed to a crystal form with very large external pores. This structure was observed for S/NiAl$_2$O$_4$ (ϕ = 2) nanocatalyst with many porosities on the surface of the support. However, S/NiAl$_2$O$_4$ (ϕ = 1.5) shows warm and plate-like particles that some of them was not thoroughly grown. Moreover, the uniform dispersion of sulfate groups is detected on all particle surfaces.

EDS analysis

The EDS analysis of the S/NiAl$_2$O$_4$ (ϕ = 1.5) is presented in Fig. 7. The sample contains Ni, Al, S, and O elements and no impurity appears the structure of the nanocatalyst. The elemental percentage of S/NiAl$_2$O$_4$ (ϕ = 1.5) shows a high similarity between gel and the final product, confirming well formation of spinel NiAl$_2$O$_4$ during combustion reaction and good bonding of sulfate groups with the surface via impregnation method.

Catalytic activity of S/NiAl$_2$O$_4$ nanocatalysts in the esterification reaction

The catalytic activity of sulfated spinel nickel aluminate prepared by different fuel amount during combustion reaction was evaluated in the esterification reaction of oleic acid (Fig. 8). As can be seen from XRD and FTIR analyses, the catalytic activity was increased because of the increase in the crystallinity of the support and increase in the bonding of the sulfate group with the surface of the catalyst. The conversion increased from 67.4% to 95.2% by increasing ϕ (fuel-to-oxidizer ratio in the combustion process) from 0.5 to 2.

However, the activity of the catalyst was changed negligibly by loading fuel more than ϕ = 1.5 (the conversion increased from 96.4% to 95.2%). Therefore, S/NiAl$_2$O$_4$ (ϕ = 1.5) nanocatalyst can be selected as an optimum catalyst for using in the biodiesel production process and further investigation.

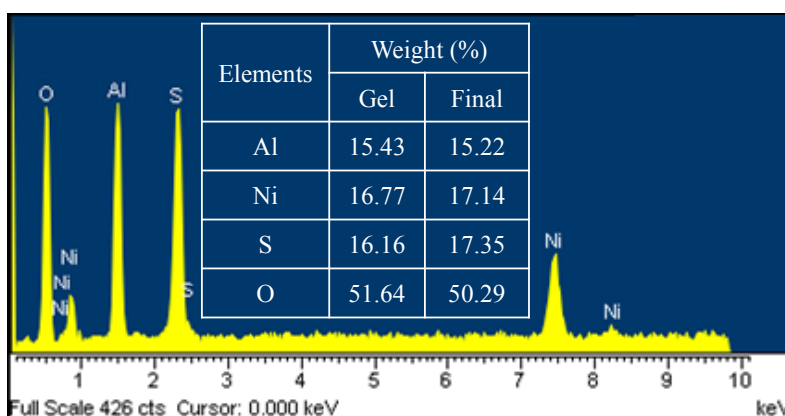| Elements	Weight (%)	
	Gel	Final
Al	15.43	15.22
Ni	16.77	17.14
S	16.16	17.35
O	51.64	50.29

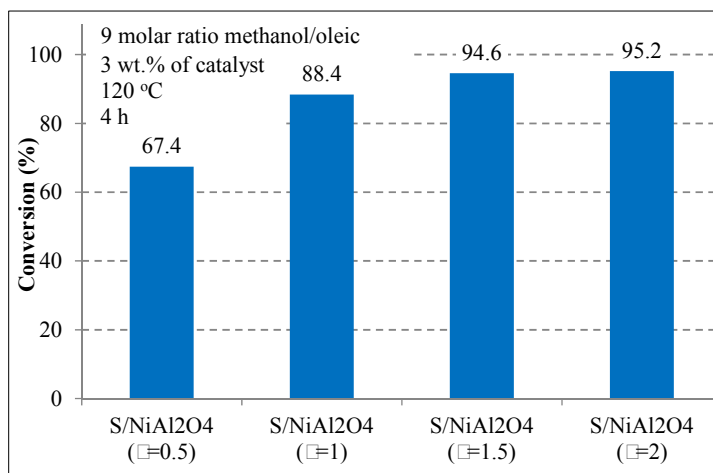Fig. 7. EDS analysis of S/NiAl$_2$O$_4$ (ϕ=1.5) nanocatalyst

Fig. 8. Activity of sulfated NiAl$_2$O$_4$ prepared by solution combustion method at different F/O ratio in the esterification reaction

Optimization of esterification reaction conditions

The esterification reaction conditions such as reaction temperature, methanol-to-oleic acid ratio, catalyst amount, and reaction time were evaluated to optimize the reaction conditions (Table 2). Evaluation of the reaction temperature shows that the conversion increased by raising the temperature from 90℃ to 135℃ due to increasing the reaction rate. However, no significant difference in the conversion was obtained for the reaction temperature of 120℃ and 135℃.

Assessment of the methanol/oleic acid ratio exhibits that the highest conversion was obtained as the ratio of 6. An increase in the methanol content moves the reaction in the forward direction. However, the solubility of methanol in biodiesel and by-product layer increases the separation cost and inactivates the catalyst by fouling its porosities, which lead to reducing the conversion. Thus, 6 molar ratio of methanol-to-oleic acid was selected as optimum.

The effect of catalyst concentration on the conversion of oleic acid to its ester was examined

by varying the amount of catalyst from 1 wt.% to 4 wt.%. The result reveals the increase in the conversion due to increasing the available active phase to make bonds between reactants. However, the conversion was not changed by loading the nanocatalyst more than 3 wt.%.

Clearly, prolonging the reaction time leads to increase the conversion because the reactants have more time to react with each other until the reaction reaches an equilibrium point. Although the conversion was sharply increased from 32.6% to 94.2% by increasing the reaction time, the conversion presented less increase by more reaction time. Therefore, 3 h was chosen as optimum to receive to equilibrium point of esterification reaction, which was performed by S/NiAl$_2$O$_4$ (ϕ = 1.5) nanocatalyst at the optimum conditions of 120℃, 6 molar ratio of methanol/oleic, acid and 3 wt.% of catalyst.

Reusability of S/NiAl$_2$O$_4$ (F/O=1.5) nanocatalyst

The reusability of S/NiAl$_2$O$_4$ (ϕ=1.5) nanocatalyst was examined in the esterification reaction under

Table 2. Optimization of esterification reaction conditions catalyzed by S/NiAl$_2$O$_4$ (F/O=1.5) nanocatalyst

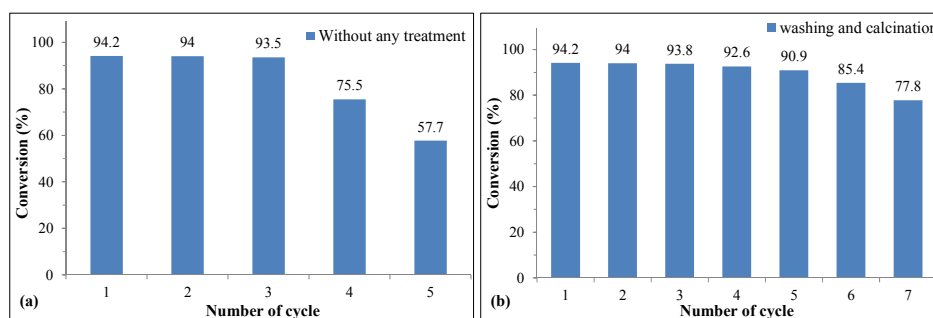| Run	Temperature (°C)	Methanol/oleic acid molar ratio	Catalyst amount (wt.%)	Reaction time (h)	Conversion (%)
1	90	9	3	4	19.2
2	105	9	3	4	52.1
3	120	9	3	4	94.6
4	135	9	3	4	95.0
5	150	9	3	4	94.9
6	120	3	3	4	84.1
7	120	6	3	4	94.5
8	120	12	3	4	94.1
9	120	15	3	4	88.2
10	120	6	1	4	48.6
11	120	6	2	4	92.8
12	120	6	4	4	94.5
13	120	6	2	1	32.6
14	120	6	2	2	84.0
15	120	6	2	3	94.2
16	120	6	2	5	94.8

Fig. 9. Reusability of S/NiAl$_2$O$_4$ (ϕ=1.5) nanocatalyst in the esterification reaction (a) without any treatment and (b) with washing and calcination after each run

optimum conditions. For this purpose, the catalyst was separated from the reaction mixture by settling and reused for the next reaction without any treatment. This process was performed after each run. The results of catalyst reusability (stability) are depicted in Fig. 9. The conversion almost was stable for three applications and then dropped sharply. Although its stability was much more than other studied nanocatalysts, further studies were performed to obtain the main reason for declining the activity [42 , 43]. This decrease can be attributed to three reasons: (1) leaching of sulfate groups from the surface of a catalyst in the reaction medium, (2) blocking the porosities of the sample and reduction the surface area, and (3) poisoning of the active phases of the catalyst by reactants and products (especially water) [16]. To evaluate the major problem for reduction the activity, the catalyst was washed twice with methanol and calcined at 550℃ for 1 h after each run. The results presented that the reusability of catalyst increased 3-5 times and then the conversion was decreased. This phenomenon revealed that although all of the mentioned reasons had an influence on the reduction the activity of the catalyst, blocking of porosities and poisoning of the active phases of S/NiAl$_2$O$_4$ ($\phi = 1.5$) nanocatalyst were the more significant ones.

CONCLUSION

Fabrication of a catalyst with high activity and stability is one of the challenges for researchers and industries. Heterogeneously biodiesel production process is one the important process for reducing the problem of petroleum fuel consumption. Considering the use of low-cost oil as feedstock in this process, many solid acid catalysts are extremely studied in this process to obtain a catalyst with the best properties and performance. In the present study, spinel nickel aluminate as stable support was prepared by a simple and cost-effective solution combustion method. Next, the effect of fuel amount of the structural and performance of its support modified by sulfate group in the esterification reaction was evaluated. The results show that excess fuel ($\phi = 1.5$) is required to obtain NiAl$_2$O$_4$ nanocatalyst with well-crystallinity, pore size, volume, well-shaped particles, and appropriate diffusion of nickel cations into alumina lattice. Using an excessive amount of fuel caused a high reduction in the material to form alpha alumina and Ni. S/NiAl$_2$O$_4$ ($\phi = 1.5$) such that the best nanocatalyst was utilized in the esterification

reaction and converted 94.2% of oleic acid to biodiesel at the optimum conditions of 120℃, 6 molar ratio of methanol/oleic acid, 3 wt.% of catalyst, and 3 h reaction time. The nanocatalyst presented high stability, at least for five uses that makes it suitable for industrial application.

CONFLICT OF INTEREST

The authors declare that there is no conflict of interests regarding the publication of this manuscript.

REFERENCES

[1] A.B. Chhetri, M.S. Tango, S.M. Budge, K.C. Watts and M.R. Islam, International Journal of Molecular Sciences, 9, 169 (2008).

[2] N.A. Negm, G.H. Sayed, F.Z. Yehia, O.I. Habib and E.A. Mohamed, Journal of Molecular Liquids, 234, 157 (2017).

[3] G. Baskar, I. Aberna Ebenezer Selvakumari and R. Aiswarya, Bioresource Technology, 250, 793 (2018).

[4] P. Nautiyal, K.A. Subramanian and M.G. Dastidar, Fuel Processing Technology, 120, 79 (2014).

[5] J. Gardy, A. Osatiashtiani, O. Céspedes, A. Hassanpour, X. Lai, A.F. Lee, K. Wilson and M. Rehan, Applied Catalysis B: Environmental, 234, 268 (2018).

[6] S. Gopinath, P.S.M. Kumar, K.A.Y. Arafath, K.V. Thiruvengadaravi, S. Sivanesan and P. Baskaralingam, Fuel, 203, 488 (2017).

[7] S.R. Setayesh, E. Abolhasani and S. Ghasemi, Progress in Reaction Kinetics and Mechanism, 41, 57 (2016).

[8] N. Mansir, Y.H. Taufiq-Yap, U. Rashid and I.M. Lokman, Energy Conversion and Management, 141, 171 (2017).

[9] A. Ashok, L.J. Kennedy and J.J. Vijaya, Journal of Alloys and Compounds, 780, 816 (2019).

[10] A. Wang, J. Wang, C. Lu, M. Xu, J. Lv and X. Wu, Fuel, 234, 430 (2018).

[11] J. Zygmuntowicz, A. Miazga, Ł. Kamiński and K. Konopka, Applied Mechanics and Materials, 797, 391 (2016).

[12] K. Nuithitikul, W. Prasitturattanachai and W. Hasin, Energy Procedia, 138, 75 (2017).

[13] K. Nuithitikul, W. Prasitturattanachai, International Journal of Green Energy, 11, 1097 (2014).

[14] H.-S. Roh, I.-H. Eum, D.-W. Jeong, B.E. Yi, J.-G. Na and C.H. Ko, Catalysis Today, 164, 457 (2011).

[15] Y. Xu, T. Wang, L. Ma, Q. Zhang and L. Wang, Biomass and Bioenergy, 33, 1030 (2009).

[16] W. Hesti, D. Apinya, The Canadian Journal of Chemical Engineering, 94, 81 (2016).

[17] A. Keskin, M. Gürü and D. Altıparmak, Fuel, 86, 1139 (2007).

[18] M. Ranjeh;, M. Mousavi-Kamazani, Journal of Nanoanalysis, 5, 249 (2018).

[19] A. Gholizadeh, Journal of Nanoanalysis, 5, 7 (2018).

[20] A. Seyed Shariatdoost, M. Yousefi, P. Derakhshi, A. Safekordi and K. Larijani, Journal of Nanoanalysis, 5, 1 (2018).

[21] M. Hashemzehi, N. Saghatoleslami and H. Nayebzadeh, Chemical Engineering Communications, 204, 415 (2016).

[22] B. Rahmani Vahid, M. Haghighi, Energy Conversion and Management, 126, 362 (2016).

[23] S. Alaei, M. Haghighi, J. Toghiani and B. Rahmani Vahid, Industrial Crops and Products, 117, 322 (2018).

[24] H. Ajamein, M. Haghighi, Energy Conversion and Management, 118, 231 (2016).

[25] B. Ye, F. Qiu, C. Sun, Y. Li and D. Yang, Journal of Chemical Technology & Biotechnology, 89, 988 (2014).

[26] C.-C. Huang, C.-J. Yang, P.-J. Gao, N.-C. Wang, C.-L. Chen and J.-S. Chang, Green Chemistry, 17, 3609 (2015).

[27] J.K. Satyarthi, S. Radhakrishnan and D. Srinivas, Energy & Fuels, 25, 4106 (2011).

[28] K. Shih, J.O. Leckie, Journal of the European Ceramic Society, 27, 91 (2007).

[29] Y. Gao, F. Meng, X. Li, J.Z. Wen and Z. Li, Catalysis Science & Technology, 6, 7800 (2016).

[30] E. Leal, L.S. Neiva, J.P.L.M.L. Sousa, F. Argolo, H.M.C. Andrade, A.C.F. de Melo Costa and L. Gama, Materials Science Forum, 660-661, 916 (2010).

[31] H. Nayebzadeh, N. Saghatoleslami, M. Haghighi and M. Tabasizadeh, Journal of the Taiwan Institute of Chemical Engineers, 75, 148 (2017).

[32] J. Zygmuntowicz, P. Wiecińska, A. Miazga and K. Konopka, Journal of Thermal Analysis and Calorimetry, 125, 1079 (2016).

[33] C.G. Anchieta, L. Tochetto, H.B. Madalosso, R.D. Sulkovski, C. Serpa, M.A. Mazutti, A.R.F.d. Almeida, A. Gündel and E.L. Foletto, Cerâmica, 61, 477 (2015).

[34] C. Ragupathi, J.J. Vijaya and L.J. Kennedy, Journal of Saudi Chemical Society, 21, S231 (2017).

[35] H. Zhang, H. Li, H. Pan, A. Wang, S. Souzanchi, C. Xu and S. Yang, Applied Energy, 223, 416 (2018).

[36] Y. Luo, Z. Mei, N. Liu, H. Wang, C. Han and S. He, Catalysis Today, 298, 99 (2017).

[37] G.-l. Shi, F. Yu, X.-l. Yan and R.-f. Li, Journal of Fuel Chemistry and Technology, 45, 311 (2017).

[38] B. Rahmani Vahid, N. Saghatoleslami, H. Nayebzadeh and J. Toghiani, Journal of the Taiwan Institute of Chemical Engineers, 83, 115 (2018).

[39] Q. Zhang, H. Li and S. Yang, Journal of Oleo Science, 67, 579 (2018).

[40] H. Nayebzadeh, N. Saghatoleslami, M. Haghighi, M. Tabasizadeh and E. Binaeian, Comptes Rendus Chimie, 21, 676 (2018).

[41] S.C. Laha, P. Mukherjee, S.R. Sainkar and R. Kumar, Journal of Catalysis, 207, 213 (2002).

[42] C.O.P. Teixeira, K.C.N.R. Pedro, T.L.A.P. Fernandes, C.A. Henriques and F.M.Z. Zotin, Chemical Engineering Communications, 1 (2018).

[43] S. Dehghani, M. Haghighi, Ultrasonics Sonochemistry, 35, 142 (2017).